Electronic Supplementary Material (ESI) for Catalysis Science & Technology.


Supporting Information

# $MnO_2$-Graphene-Oxide-Scroll-$TiO_2$ Composite Catalyst for Low-Temperature $NH_3$-SCR of NO with Good Steam and $SO_2$ Resistance Obtained by Low-Temperature Carbon-Coating and Selective Atomic Layer Deposition

Liwei Sun,[a,b] Kai Li,[a,b] Zeshu Zhang,[a,b] Xuefeng Hu,[a] Heyuan Tian,[a,b] Yibo Zhang*[a] and Xiangguang Yang*[a,b]
[a] State Key Laboratory of Rare Earth Resource Utilization, Jilin Province Key Laboratory of Green Chemistry and Process, Changchun Institute of Applied Chemistry, Chinese Academy of Science, Changchun 130022, China
[b] University of Science and Technology of China, Hefei 230026, China

## 1. Computational Details

The calculations were carried out using density functional theory (DFT) with the Perdew-Burke-Ernzerbof (PBE) form of generalized gradient approximation functional (GGA).[1] The Vienna ab-initio simulation package (VASP) was employed.[2-5] The plane wave energy cutoff was set as 400 eV. The Fermi scheme was employed for electron occupancy with an energy smearing of 0.1 eV. The first Brillouin zone was sampled in the Monkhorst−Pack grid.[6] The 3×3×1 k-point mesh for the surface calculation. The energy (converged to $1.0 \times 10^{-6}$ eV/atom) and force (converged to 0.01eV/Å) were set as the convergence criterion for geometry optimization. The spin polarization was considered in all calculation. To accurately describe the van der Waals (vdW) interaction involved in graphene, the semiempirical DFT-D2 force-field approach was employed in this study.[7]

The (110) surface of $MnO_2$ is obtained by cutting the $MnO_2$ bulk along {110} directions. In the structural optimization calculation for $MnO_2$(110), the atoms of the bottom layer are fixed, while the positions of the other atoms were allowed to relax. However, for graphene, all the atoms were allowed to relax. A vacuum layer as large as 15 Å was used along the C direction normal to the surfaces to avoid periodic interactions.

## 2. Additional Figures

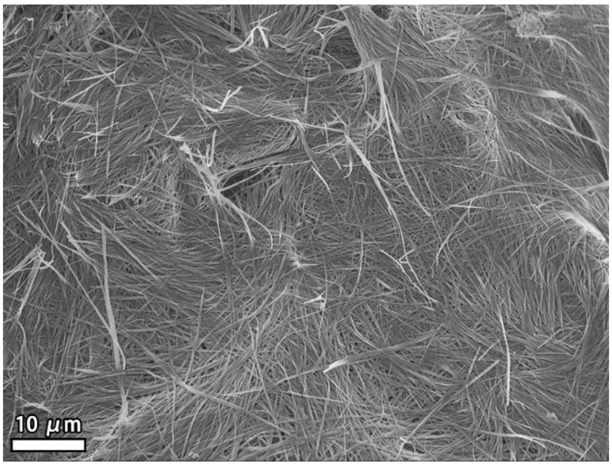


**Figure S1.** Morphology characterization: SEM image of $MnO_2$-GOS-$TiO_2$.

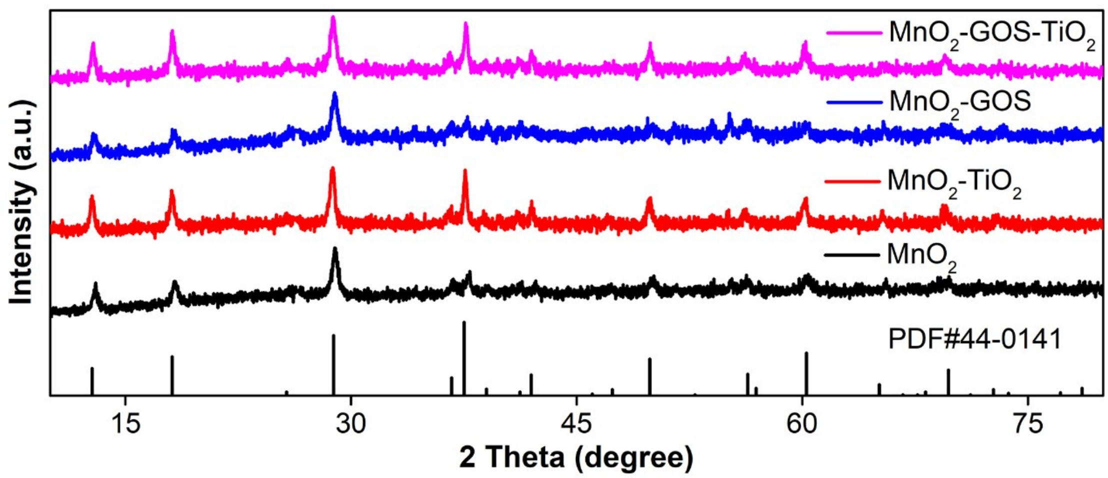


**Figure S2**. Structural characterization, XRD pattern of $MnO_2$, $MnO_2$-$TiO_2$, $MnO_2$-GOS and $MnO_2$-GOS-$TiO_2$.

The diffraction peaks located at 13 ° could be assigned to the (110) characteristic diffraction of the $MnO_2$. The surface spacing of this crystal plane was consistent with that measured by HRTEM image in Figure 2d.

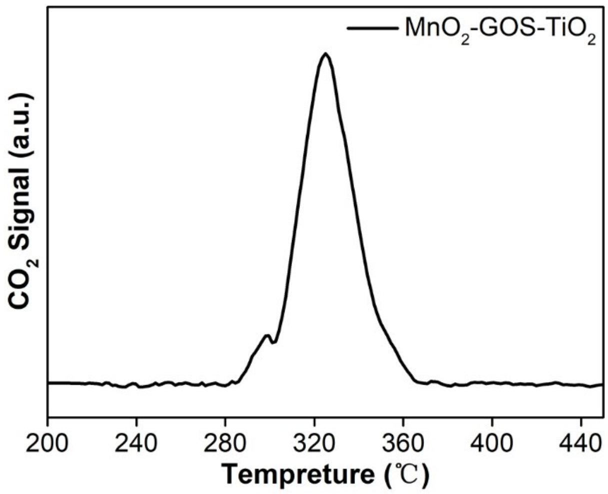


**Figure S3.** The temperature-programmed oxidation (TPO) of GO in reaction atmosphere.

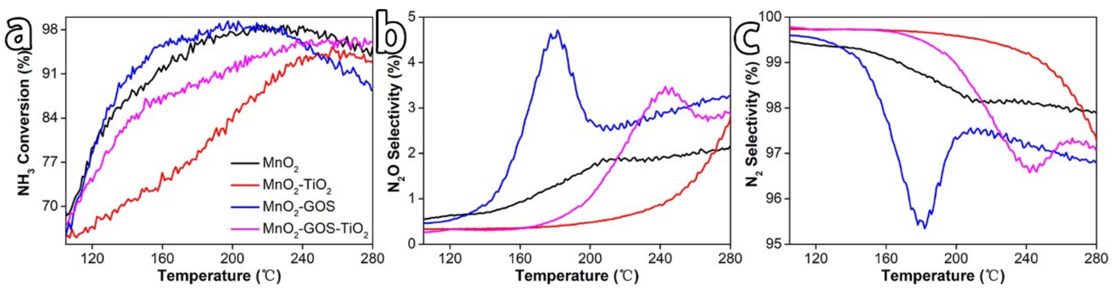


**Figure S4.** Catalyst performance: (a) $NH_3$ conversion, (b) $N_2O$ selectivity and (c) $N_2$ selectivity of $MnO_2$, $MnO_2$-$TiO_2$, $MnO_2$-GOS and $MnO_2$-GOS-$TiO_2$ (content of $TiO_2$ in $MnO_2$-$TiO_2$ was 0.2 %, content of C in $MnO_2$-GOS was 2 %, $TiO_2$ and C content of $MnO_2$-GOS-$TiO_2$ were the same as the first two) in the presence of steam.

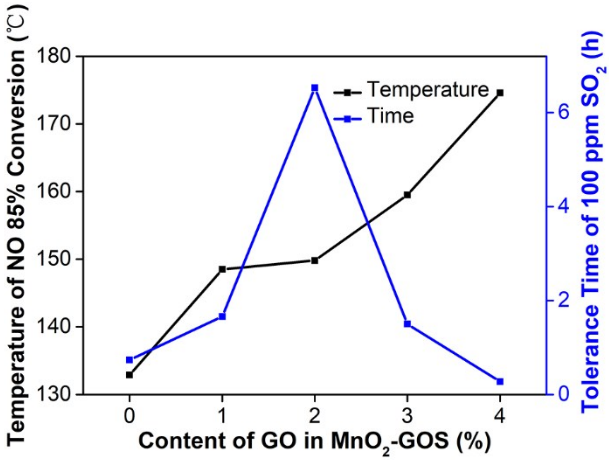


**Figure S5.** Relationship between catalyst performance and content of GO in $MnO_2$-GOS.

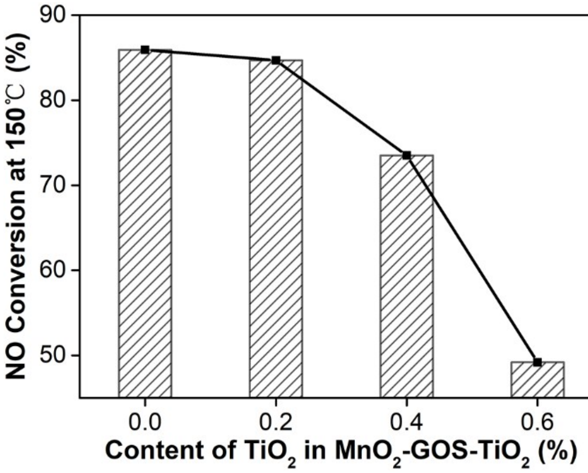


**Figure S6.** Relationship between catalyst performance and content of $TiO_2$ in $MnO_2$-GOS-$TiO_2$.

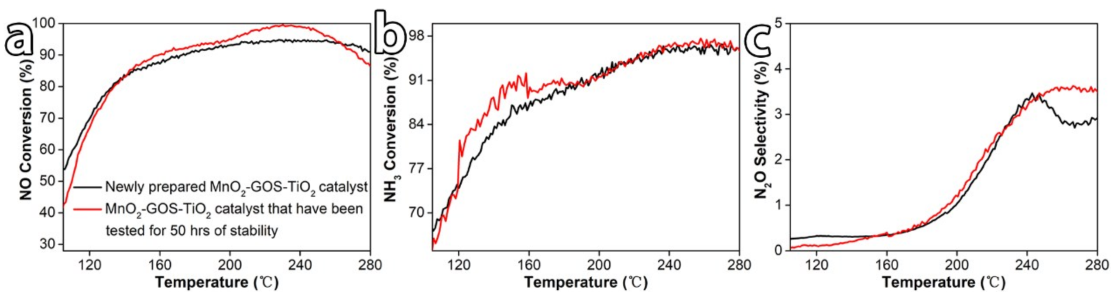


**Figure S7.** Catalyst performance:(a) NO conversion, (b) $NH_3$ conversion and (c) $N_2O$ selectivity of newly prepared and used $MnO_2$-GOS-$TiO_2$ catalyst in the presence of steam.

**Table S1.** Rates and turnover frequencies of $NH_3$-SCR[a]

| | Rate of reaction ($10^{-7}$ mol $g^{-1}$ $s^{-1}$) | | | TOF[c] ($10^{-3}$ $s^{-1}$) | |
|---|---|---|---|---|---|
| Catalyst (D)[b] | Overall | Complete reduction ($N_2$) | Partial reduction ($N_2O$) | Overall | Complete reduction ($N_2$) |
| $MnO_2$ (1.52) | 5.6 | 5.2 | 0.4 | 3.2 | 3.0 |
| $MnO_2$-$TiO_2$ (0.37) | 5.1 | 4.8 | 0.3 | 12 | 11.3 |
| $MnO_2$-GOS (0.69) | 5.6 | 5.2 | 0.4 | 7.1 | 6.6 |
| $MnO_2$-GOS-$MnO_2$ (0.58) | 5.5 | 5.3 | 0.2 | 8.2 | 7.9 |

[a] 500 ppm NO reacted after 10 mins at 150 °C in the presence of the steam and $SO_2$.

[b] Dispersion values in percent were given in parentheses.

[c] Turnover frequencies with respect to the surface atoms.

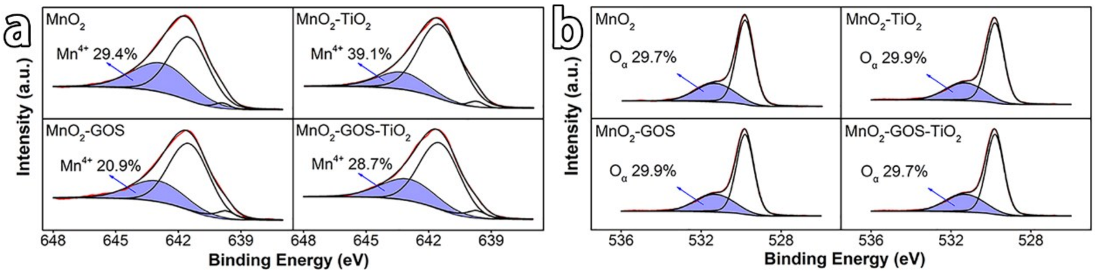


**Figure S8.** XPS spectra for (a) Mn $2p_{3/2}$ and (b) O $2p_{3/2}$ for $MnO_2$, $MnO_2$-$TiO_2$, $MnO_2$-GOS and $MnO_2$-GOS-$TiO_2$.

| **Entry** | **Procedure** | **Gas Fluid** | **Catalyst** |
|---|---|---|---|

| | | | $MnO_2$ | $MnO_2$-$TiO_2$ | $MnO_2$-GOS | $MnO_2$-GOS-$TiO_2$ |
|---|---|---|---|---|---|---|
| **1** | He-280°C -30mins-30°C<br>$NO+O_2$-30mins<br>He-30mins<br>He-warming up and recording<br>50°C, 100°C, 150°C, 200°C, 250°C | He<br>$NO+O_2$<br>He | Figure S9a | Figure S9b | Figure S9c | Figure 7a |
| **2** | He-280°C -30mins-30°C<br>$NH_3$-30mins<br>He-30mins<br>He-warming up and recording<br>50°C, 100°C, 150°C, 200°C, 250°C | He<br>$NH_3$<br>He | Figure S9d | Figure S9e | Figure S9f | Figure 7b |
| **3** | He-280°C -30mins-50°C<br>$NH_3$-30mins<br>He-30mins<br>$NO+O_2$-50°C -recording<br>0min, 0.5mins, 1.5mins, 5mins, 8mins | He<br>$NH_3$<br>He<br>$NO+O_2$ | Figure S9g | Figure S9h | Figure S9i | Figure 7c |
| **4** | He-280°C -30mins-150°C<br>$NO+O_2$-30mins<br>He-30mins<br>NH3-150°C -recording<br>0min, 0.5mins, 1.5mins, 5mins, 8mins | He<br>$NO+O_2$<br>He<br>$NH_3$ | Figure S9j | Figure S9k | Figure S9l | Figure 7d |
| **5** | He-280°C -30mins-30°C<br>$NO+O_2+NH_3$-30mins<br>$NO+O_2+NH_3$-warming up and recording<br>50°C, 100°C, 150°C, 200°C, 250°C | He<br>$NO+O_2+NH_3$ | Figure S9m | Figure S9n | Figure S9o | Figure 7e |

**Table S2.** DRIFT study on mechanism of $NH_3$-SCR

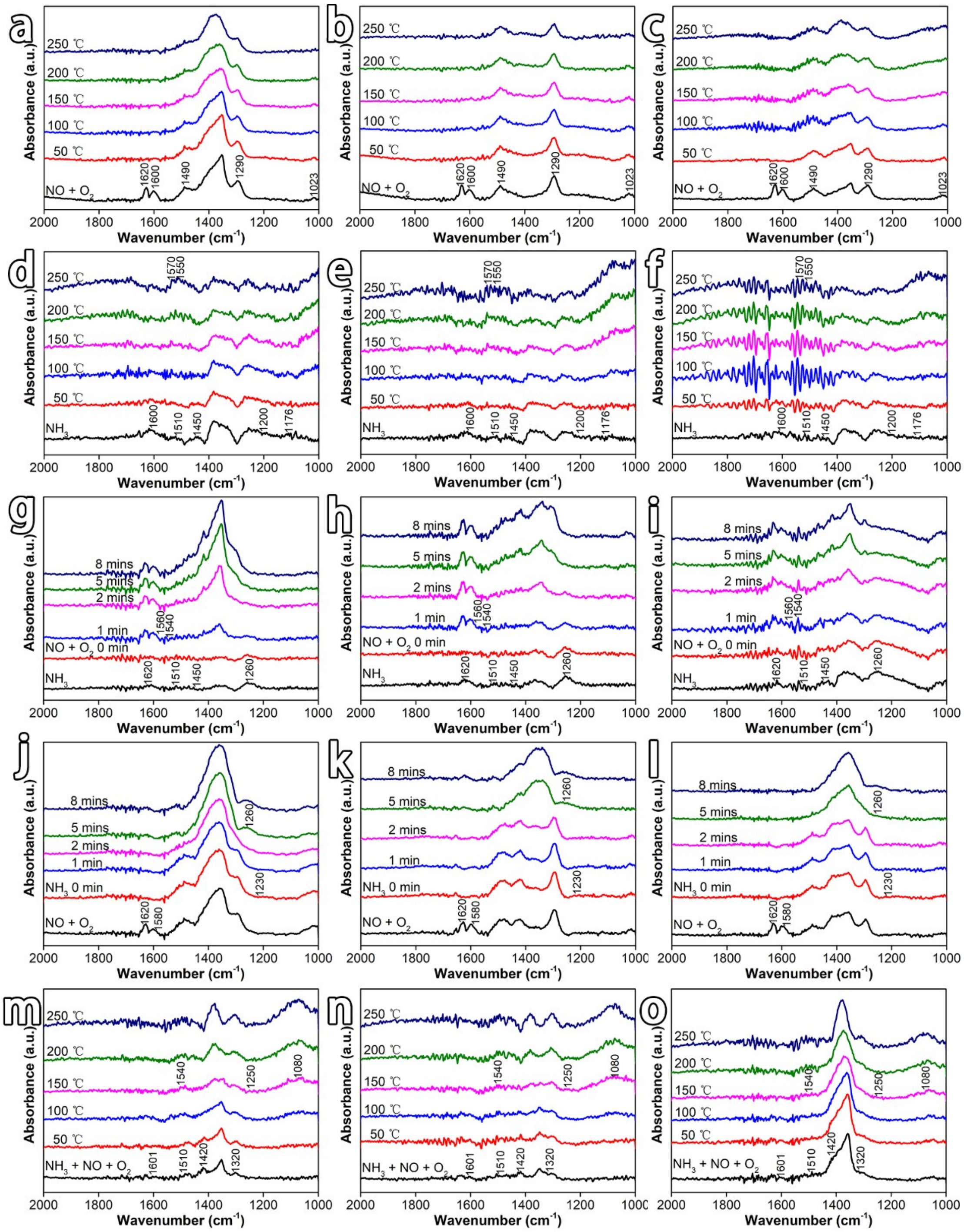


**Figure S9.** DRIFT study on $NH_3$-SCR mechanism of $MnO_2$, $MnO_2$-$TiO_2$ and MnO2-GOS-$TiO_2$.

## 3. Reference

[1] J. P. Perdew, K. Burke, M. Ernzerhof Generalized gradient approximation made simple, Phys. Rev. Lett. 77 (1996) 3865-3868.

[2] G. Kresse, J. Furthmüller, Efficiency of ab-initio total energy calculations for metals and semiconductors using a plane-wave basis set, Comp. Mater. Sci. 6 (1996) 15-50.

[3] G. Kresse, J. Hafner, Ab initio molecular dynamics for liquid metals, Phys. Rev. B 47 (1993) 558-561.

[4] G. Kresse, J. Hafner, Ab initio molecular-dynamics simulation of the liquid-metal–amorphous-semiconductor transition in germanium, Phys. Rev. B 49 (1994) 14251-14269.

[5] G. Kresse, J. Furthmüller, Efficient iterative schemes for ab initio total-energy calculations using a plane-wave basis set, Phys. Rev. B 54 (1996) 11169-11186.

[6] H. J. Monkhorst, J. D. Pack, Special points for brillouin-zone integrations, Phys. Rev. B 13 (1976) 5188-5192.

[7] G. Henkelman, B. P. Uberuaga, H. Jónsson, A climbing image nudged elastic band method for finding saddle points and minimum energy paths, J. Chem. Phys. 113 (2000) 9901-9904.